Mars sub-millimeter sensor on micro-satellite: sensor feasibility study

Richard Larsson[1,6], Yasuko Kasai[1], Takeshi Kuroda[1], Shigeru Sato[1], Takayoshi Yamada[1], Hiroyuki Maezawa[2], Yutaka Hasegawa[3], Toshiyuki Nishibori[4], Shinichi Nakasuka[5], and Paul Hartogh[6]

[1]National Institute of Information and Communications Technology, Tokyo, Japan
[2]Osaka Prefecture University, Osaka, Japan
[3]Institute of Space and Astronautical Science, Japanese Aerospace Exploration Agency, Tokyo, Japan
[4]Research and Development Directorate, Japanese Aerospace Exploration Agency, Tokyo, Japan
[5]Tokyo University, Tokyo, Japan
[6]Max Planck Institute of Solar System Research, Göttingen, Germany

Correspondence to: Richard Larsson (larsson@mps.mpg.de)

Abstract. We present a feasibility study for a sub-millimeter instrument on a small Mars platform now under construction. The sensor will measure the emission from atmospheric molecular oxygen, water, ozone, and hydrogen peroxide in order to retrieve their volume mixing ratios and the changes therein over time. In addition to these, the instrument will be able to limit the crustal magnetic field, and retrieve temperature and wind speed with various degrees of precision and resolution. The expected measurement errors before spatial and temporal averaging are 15 ppmv to 25 ppmv for the molecular oxygen mixing ratio, 0.2 ppmv for the gaseous water mixing ratio, 2 ppbv for the hydrogen peroxide mixing ratio, 2 ppbv for the ozone mixing ratio, $1.5\,\mu\mathrm{T}$ to $2.5\,\mu\mathrm{T}$ for the magnetic field strength, $1.5\,\mathrm{K}$ to $2.5\,\mathrm{K}$ for the temperature profile, and $20\,\mathrm{m\,s^{-1}}$ to $25\,\mathrm{m\,s^{-1}}$ for the horizontal wind speed.

1 Introduction

We are building a sub-millimeter sensor with aim towards Mars using a micro-satellite platform. The goal is to launch in 2024, and the main scientific target is to measure changes in Martian molecular oxygen over time. The sensor is based on a previous proposal of a more advanced version of the instrument by Kasai et al. (2012), and our working name for the sensor and platform is the Terahertz Experiment (TEREX). As both Urban et al. (2005) and Kasai et al. (2012) has previously suggested, the advantages of sub-millimeter technology for Martian remote sensing is that the radiation at sub-millimeter frequencies are mostly unaffected by atmospheric dust content, and that the radiation observed is passively emitted by the target atmospheric gases. The sensor will be able to measure molecular oxygen, gaseous water, hydrogen peroxide, ozone, the temperature field, the wind field, and the strongest crustal magnetic fields. These observations are possible from radiation emitted from within dust storms, and are independent of the local time.

Martian molecular oxygen has been measured several times by missions like Viking, Herschel, Curiosity, and MAVEN. Carleton and Traub (1972) measured a global molecular oxygen profile of 1300 ppmv, Hartogh et al. (2010) measured a constant 1400 ppmv profile in whole disk measurements but remarked that there could be a higher concentration near the surface,

Mahaffy et al. (2013) measured a constant profile of 1450 ppmv in ground-based measurements, and Sandel et al. (2015) measured up to 4000 ppmv at altitudes of 90 to 120 km in limb measurements at nanometer wavelengths. The discrepancies are small between most of these, but are important and should be studied in more details. Molecular oxygen acts as the chemical background that oxidizes gaseous water and various hydrogen radicals. Low altitude variations have not been measured in detail over time. The Sandel et al. (2015) results shows that the profile cannot be constant from the ground up to 90 km, so the volume mixing ratio must increase in some altitude range. Our sensor will not be able to confirm these measurements because the altitude range of Sandel et al. (2015) is above our reach. The instrument we describe here will be able to see if the increase observed at 90 km are reflected near the surface, and limit the altitude range at which the relative oxygen concentration starts increasing. Another of the key features of Mars that our sensor can help with is to measure some limited dust storm-induced chemistry. Dust storms can have large electric fields, which means that there will be a large increase in hydrogen peroxide when these storms are active (as suggested in the works by, e.g., Delory et al., 2006; Atreya et al., 2006). Since sub-millimeter waves are barely affected by atmospheric dust, the instrument will be able to sense hydrogen peroxide production inside the dust cloud.

This paper is dedicated to show the feasibility study we performed to test the sensor design of TEREX. There will be other papers about the mission to describe the details of the orbit insertion and retention, and to give a broader scientific overview of the mission as a whole. This paper shows the forward simulations of the expected observations, and the error estimations from a simple retrieval setup. The next section describes the method of how we set up our simulations — it also discusses some of the limitations that we have encountered. After the description of our method, we show our results, discuss their consequences, and give our concluding remarks.

2 Method

This section goes through the basic assumptions we made to perform the simulations. This includes orbit considerations, sensor design, spectroscopic modeling, and retrieval procedure.

2.1 Orbit

The sub-millimeter sensor will be carried to Mars on a satellite weighing less than 100 kg. Such a small satellite needs special means to enter orbit. The selected method to achieve orbit is to use the atmospheric drag to perform aerocapture. Aerocapture has never been attempted successfully before — as far as we are aware — so final orbital parameters are to some extent uncertain. A future work will discuss the orbit insertion and retention in details. For this work, we have opted to work simply with two sets of observations taken from an orbit with the Kepler elements semi-major axis of $6150\,\mathrm{km}$ and eccentricity of 0.5. This gives a periareion altitude of $400\,\mathrm{km}$ and an orbit time of 5 hours and 20 minutes. We will show simulated observations as well as estimated errors for retrieved atmospheric quantities in limb scanning mode near the periareion and in nadir staring mode near the apoareion. The final orbit could differ from the one above, but the feasibility of the sensor is not strictly dependent on the details of the orbit. As long as the periareion is not too high, it will merely affect its spatial resolution.

2.2 Sensor

The sensor is also limited mass and power budget by the small scale of the platform itself. We will for instance not be able to change the local oscillator to be sensitive to different ranges than those selected on the design board. A schematic sketch of the instrument can be seen in Figure 1. The spectrometer we plan to use is the chirp transform spectrometer designed for the Jupiter icy moons explorer's sub-millimeter wave instrument, with 10000 channels over a 1-GHz range (for examples on this type of spectrometer, see, e.g., Hartogh, 1997). The local oscillator will be at 481.15 GHz with a central intermediate frequency of 6 GHz. There will be no suppression of either of the sidebands, so the measured radiation will be from between 474.65-475.65 GHz and 486.65-487.65 GHz. The system noise temperature is expected to be about 2000 K in double-sideband mode. The antenna is planned to be a 30 cm large and made of carbon fiber reinforced plastic. This achieves a 10 km vertical footprint at orbit altitudes below about 400 km, with a resolution half-width of about $0.14°$. A lower system noise would improve all results presented below, though the quoted number is as good as we expect the instrument will be at time of flight.

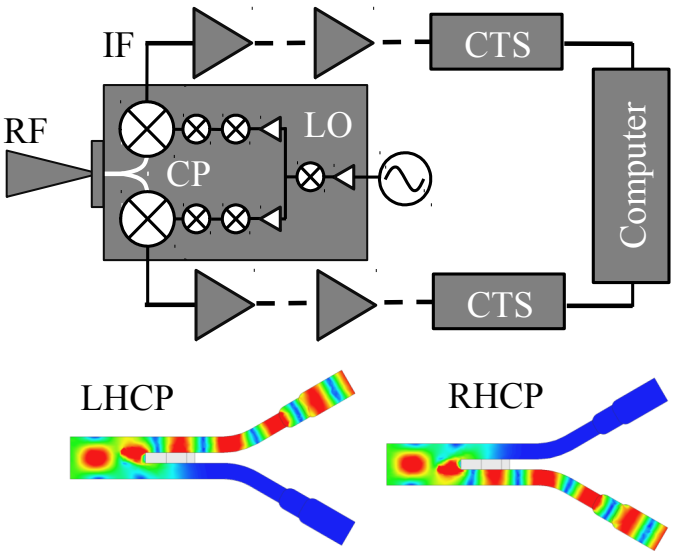

Figure 1. Sketch of sensor electronics design. The radio frequencies (RF) between 474.65-475.65 GHz and 486.65-487.65 GHz enters from the left in the figure and is split by a circular polarizer (CP) into left-handed, and right-handed, circular polarization (LHCP, RHCP) as demonstrated in the colored plots above. The signal is then mixed with the signal of a local oscillator at 481.15 GHz, to lower the frequency to a measurable range. At an intermediate frequency of 6 GHz the chirp transform spectrometer turns this analog signal into a digital signal that is fed into a computer for preparations and to be sent back to Earth.

We plan to use two identical receiver systems with the same setups but fed different states of polarization. The polarization states will be separated using a feed horn antenna. This way, if one of the receiver chains experience technical issues, we can use the other to keep measuring the atmosphere. In addition, while both chains work we can measure the magnetic field.

Molecular oxygen is affected by the Zeeman effect (Zeeman, 1897), so it is possible to sense the strongest crustal magnetic field through the state of polarization (for more details, please see Larsson et al., 2013, 2014, 2017; Larsson et al.).

Because of the dual receiver systems, if we take a single measurement every second, the measurements alone produces about 160 kbps of data before any compression is applied. This exceeds our maximum transfer rate, so we will have to perform limited data reduction on-board the spacecraft. The software for this is not ready yet. The only reduction considered in this work is an averaging by pairing immediate neighboring channels to increase the effective width of a channel to 200 kHz. This is still well below the line width of the absorption lines that we consider here, so no physics is lost.

2.3 Forward Model

We use the Atmospheric Radiative Transfer Simulator (ARTS; Eriksson et al., 2011; Buehler et al., 2018) for all forward simulations. ARTS is a fully three-dimensional model with full polarization capabilities that have been used in numerous studies. Please see the two cited articles, other articles citing them, and the source code — available via a copyleft license at `www.radiativetransfer.org` — to understand the radiative transfer method of ARTS in more details. All of the data used in this study can be found via aforementioned link.

The standard scenario atmosphere is from daytime simulations by Laboratoire de Météorologie Dynamique's global circulation model (Forget et al., 1999) for a solar angle of zero degrees. The temperature and volume mixing ratio profiles for key species are shown in Figure 2. The magnetic field is set to a constant $1\,\mu\mathrm{T}$ throughout the transfer, pointing along the line of sight of the transfer. We expect there to be a large variations in some gases (i.e., gaseous water, ozone and hydrogen peroxide), and in the strength of the magnetic field. In order to demonstrate how the error estimation changes as the forward model scenario changes, we perform the simulations at a factor 100 times less volume mixing ratio of these gases and of the magnetic field. In this reduced case, we still keep the temperature and molecular oxygen mixing ratios the same as in the standard scenario. We do not set the wind speed in any scenario but perform retrievals of it from analytical expressions of its Jacobian.

A spectroscopic suite suitable for Mars was developed by Buehler et al. (2018), which we use for our simulations. It computes pressure broadening and shifting per atmospheric species rather than from a predefined atmospheric composition. We also use the carbon dioxide collision-induced absorption from Gruszka and Borysow (1997) as a continua shown in Figure 3. This continua is key to low altitude limb measurements, and is the main reason we are focusing on the $400\,\mathrm{GHz}$ range rather than higher frequencies. Note that the continua is effectively twice as strong as normal since we will not suppress the lower or upper sidebands. A big problem with this continua is that it is only defined down to a temperature of $200\,\mathrm{K}$. For lower temperatures we simply extrapolate to these using the Gruszka and Borysow (1997) code by ignoring the warnings. Despite these issues, we still choose to include the continua since ignoring a potential 20-120 K signal would be catastrophic for the science of the mission. Clearly, the carbon dioxide continua has to be studied more for Mars atmospheric conditions since its influence is notably strong. Even if our extrapolation is the cause of most of the absorption that we see (because of some model artifact at lower temperatures), it is necessary to confirm that this is the case, and to limit the influence of the continua.

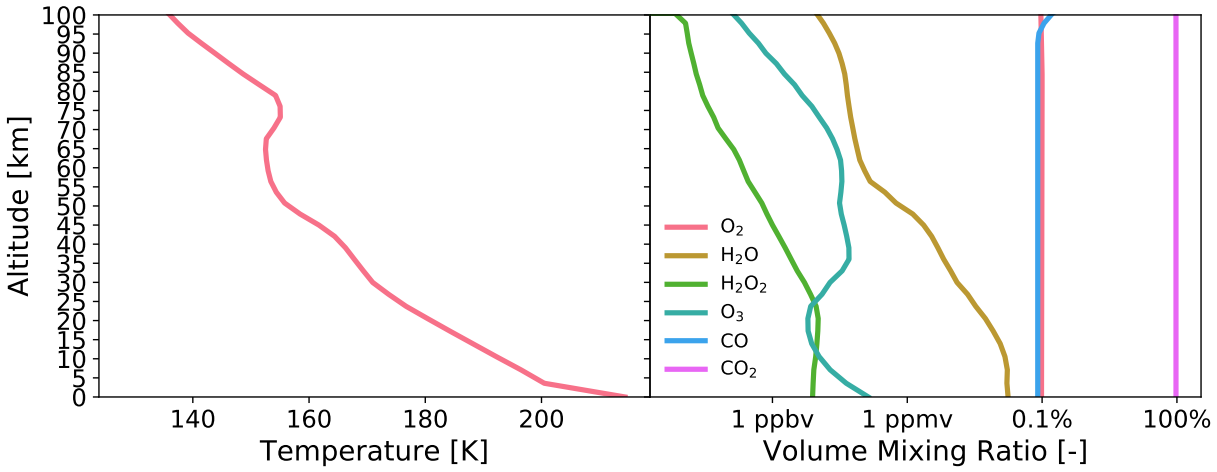

Figure 2. Temperature and volume mixing ratio profiles used in the simulations.

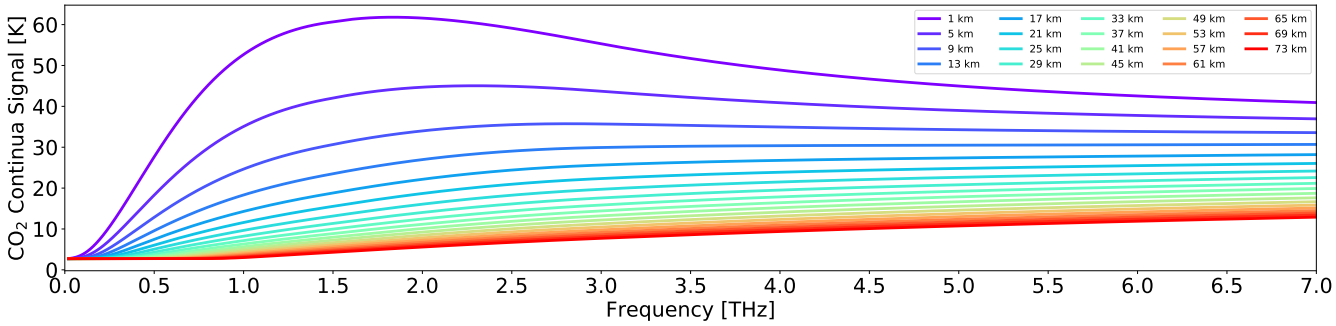

Figure 3. Limb pencil view simulation of Mars considering only the carbon dioxide continua. Pencil tangent altitudes are indicated by the legend. The increase in the signal at higher altitudes and higher frequency is probably a consequence of the extrapolation of the model parameters.

2.4 Error Analysis

We use the optimal estimation method described by Rodgers (2000) to predict at what level of precision and resolution we will be able to measure atmospheric parameters. This is done from assuming a linear error. Errors tend to be linear near the target even if the retrieval process or underlying physics is non-linear. The computed error is from

$$\mathbf{e}_x = \mathbf{S}_a \mathbf{J}^\top \left(\mathbf{J} \mathbf{S}_a \mathbf{J}^\top + \mathbf{S}_e \right)^{-1} \mathbf{e}_y, \tag{1}$$

where $\mathbf{S}_a$ is the a priori covariance matrix, $\mathbf{J}$ is the Jacobian matrix, $\mathbf{S}_e$ is a diagonal radiance error covariance matrix, and $\mathbf{e}_y$ is a Gaussian realization of the measurement error. This realization is repeated a number of times to estimate the error on retrieved parameters. The error covariance is set to be diagonal, having the square of the standard deviation of the measurement error at each point. For most of the simulations below we assume a diagonal a priori covariance matrix. For the one figure we do not

at the end, the correlation of this matrix is assumed to decrease exponentially the further the distance is from the diagonal, as described by Eriksson et al. (2005), and the correlation between retrieved parameters (i.e., wind, temperature, magnetic field strength, O_2, H_2O, H_2O_2, and O_3 volume mixing ratios) are still assumed to be zero. The a priori variance at each altitude level is from a standard deviation of the molecular oxygen mixing ratio of 100 ppmv, of the gaseous water mixing ratio of 1 ppmv, of the hydrogen peroxide and ozone mixing ratios of 10 ppbv, of the magnetic field strength of $10\,\mu\mathrm{T}$, of the temperature of $10\,\mathrm{K}$, and of the wind speed of $100\,\mathrm{m\,s^{-1}}$. These numbers were chosen because they are the closest order of magnitude standard deviations that produces a clear measurement response for each model parameter in the limb scanning simulations at $1\,\mathrm{s}$ integration time. For some of these parameters, we will discuss what happens to the error estimations by increasing the standard deviation by one order of magnitude. The measurement response is defined as

$$\mathbf{r} = \mathbf{S}_a\mathbf{J}^\top\left(\mathbf{J}\mathbf{S}_a\mathbf{J}^\top + \mathbf{S}_e\right)^{-1}\mathbf{J}\mathbf{u} = \mathbf{A}\mathbf{u}, \tag{2}$$

where $\mathbf{u}$ is a vector of ones, and $\mathbf{A}$ is the averaging kernel. We define a clear measurement response as $\max(\mathbf{r}) > 0.8$. The trace of $\mathbf{A}$ gives the degrees of freedom of the retrieval system.

Note that the shape of the averaging kernels gives the altitude range where the measurements are sensitive to the atmospheric parameters, a combination of the instrument's statistical and physical vertical resolution. The degrees of freedom of the averaging kernel gives a rough estimation of how many distinct parameters can be set over the entire profile altitude range, given the statistical constraints. A reduction in the degrees of freedom by, e.g., assuming a larger statistical correlation distance or by integrating the signal over a wider vertical slice of the atmosphere, should be followed by an increase in the precision of the retrieved parameter at the cost of a loss in vertical resolution. It is also possible to increase the precision of the retrieved model parameters by increasing the integration time to reduce the measurement noise. This has the cost of reducing the spatial resolution either vertically or horizontally. We will not consider this type of reduced resolution in this work, partly because such a reduction can be done by averaging measurements a posteriori so long as the original data is available in a high time resolution. The only test of resolution versus precision we make in this work is one where we vary the a priori correlation distance. Although a very crude estimation, it serves the purpose of finding a limit to the precision.

3 Results and Discussion

This section gives the forward simulation results and the estimated errors on the retrieved parameters. The first subsection shows the simulated signal in the frequency range we are working in. The next subsection presents the error estimates for limb scanning observations with a satellite altitude at 400 km for the presented signal and for a signal with 100 times less gaseous water, hydrogen peroxide, and ozone, and with a 100 times weaker magnetic field. The error estimations are from a one second long integration time per tangent altitude with all tangent profile used to make up the inputs to Equation 1 for the error estimations. The next subsection also presents nadir staring error estimations. We set the integration time to one hour in nadir staring mode to reduce the signal to noise ratio.

3.1 Modeled Sensor Signal

The simulated signal from $486.65\,\mathrm{GHz}$ to $487.65\,\mathrm{GHz}$ and from $475.65\,\mathrm{GHz}$ to $474.65\,\mathrm{GHz}$ is shown in Figure 4. The signal shows two hydrogen peroxide absorption lines at 475.20 GHz and 487.20 GHz, a single molecular oxygen absorption line at 487.25 GHz, a single ozone absorption line at 487.35 GHz, and a single gaseous water absorption line near the edge at 474.69 GHz. The limb view signal from molecular oxygen is saturated at the lowest tangent altitude (peaks of 95 K in the double sideband view), but its signal is much reduced at higher altitudes. The gaseous water signal is also saturated at lower tangent altitudes but weakens greatly at higher tangent altitudes. The ozone signal is weak, about 5 K in strength at low altitudes but remains about as strong at higher altitudes due to its by altitude increasing volume mixing ratio. The hydrogen peroxide signal is also weak, but much stronger than the ozone signal, at 10 K at low altitudes, but its strength decreases more rapidly at higher altitudes.

3.2 Error Estimations

The estimated errors on the forward model parameters for limb scanning observations are shown in Figures 5 for a single second of integration time pointing at each of the tangent altitudes of Figure 4. In addition to the signal in Figure 4, we also present a case in Figure 6 where the gaseous water, the hydrogen peroxide, and the ozone volume mixing ratios, as well as the magnetic field strength, are reduced by a factor 100. Below, for simplicity, the atmosphere with less water is called 'dry' and the atmosphere with more water is called 'wet'. The estimated errors on the forward model parameters for nadir staring mode are shown in Figure 7 for one full hour of integration time.

About Figure 5, Figure 6, and Figure 7,

- Molecular oxygen: Expected error levels are of 25 ppmv with good measurement response from $10\,\mathrm{km}$ to $30\,\mathrm{km}$ in limb scanning mode. In nadir staring mode, the altitude range of good measurement response extends from $10\,\mathrm{km}$ to $40\,\mathrm{km}$, and the expected error is about 15 ppmv. Molecular oxygen is not expected to change at short timescales, so either scenario is good for the purpose of the mission to limit molecular oxygen variations. Longer integration times in limb scanning mode, or staring at lower altitudes, could be useful for limiting the vertical profile of the molecule better, especially at lower altitudes. For instance, the very near-surface error achieve good measurement response by merely increasing the integration time to $2\,\mathrm{s}$ staring every $10\,\mathrm{km}$ from $5\,\mathrm{km}$ to $35\,\mathrm{km}$.

- Gaseous water: Reducing the gaseous water content increases sensitivity at lower altitudes as the line absorption is no longer saturated. In limb scanning mode, the expected error is around 0.2 ppmv, with a range of good measurement response from $40\,\mathrm{km}$ to $70\,\mathrm{km}$ for a wet atmosphere and from $10\,\mathrm{km}$ to $80\,\mathrm{km}$ in a dry atmosphere. In nadir staring mode, the measurement response is good from $10\,\mathrm{km}$ to $40\,\mathrm{km}$ with similar levels of error estimated as for the limb scanning mode. To have a good measurement response near the surface for a single profile in a wet atmosphere, the a priori standard deviation of water can be increased by an order of magnitude, which yields an error estimation of about 3 ppmv and good measurement response from ground to $40\,\mathrm{km}$.

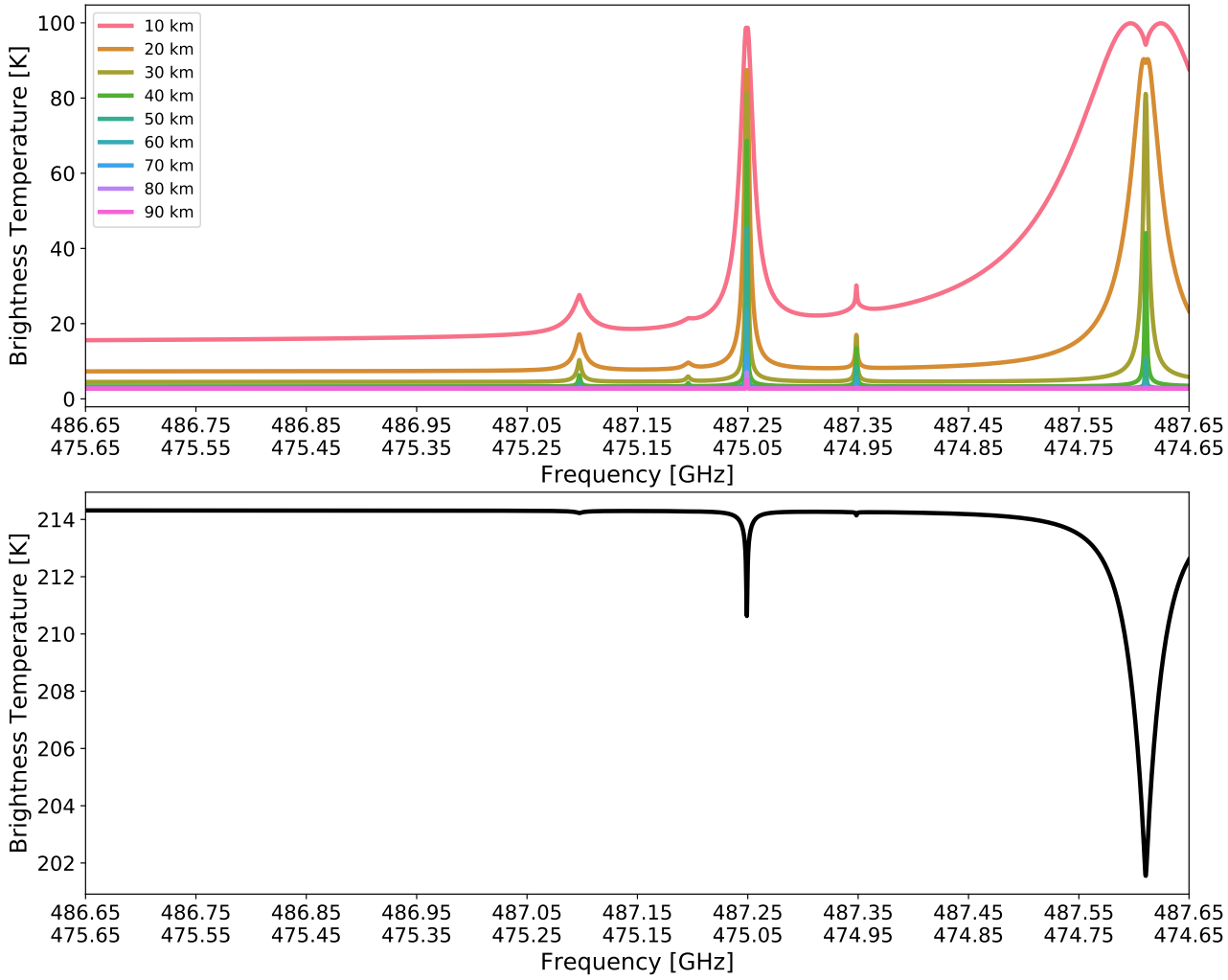

Figure 4. Simulated signal for the sensor. The signal unit is in Planck-equivalent brightness temperature as expected with the sensor calibrated to have half of its measured signal from each sideband. The upper row shows the simulated limb scanning geometry for several tangent altitudes (used in later figures). The legend contains the tangent altitudes. The lower row shows the simulated nadir staring mode signal (also used in later figures).

– Hydrogen peroxide: In limb scanning mode, hydrogen peroxide has expected errors around 2 ppbv in both wet and dry atmospheres. Also the good measurement response altitude range is from $10\,\mathrm{km}$ to $80\,\mathrm{km}$ in both scenarios. The estimated error is similar in the nadir staring mode, but the altitude range is reduced from $10\,\mathrm{km}$ to $40\,\mathrm{km}$. An estimated error of 2 ppbv is about $20\,\%$ of the total hydrogen peroxide content in the standard wet atmosphere. Since the species is expected to increase by dust storms, this error should be good enough to characterize its production and destruction inside said storms.

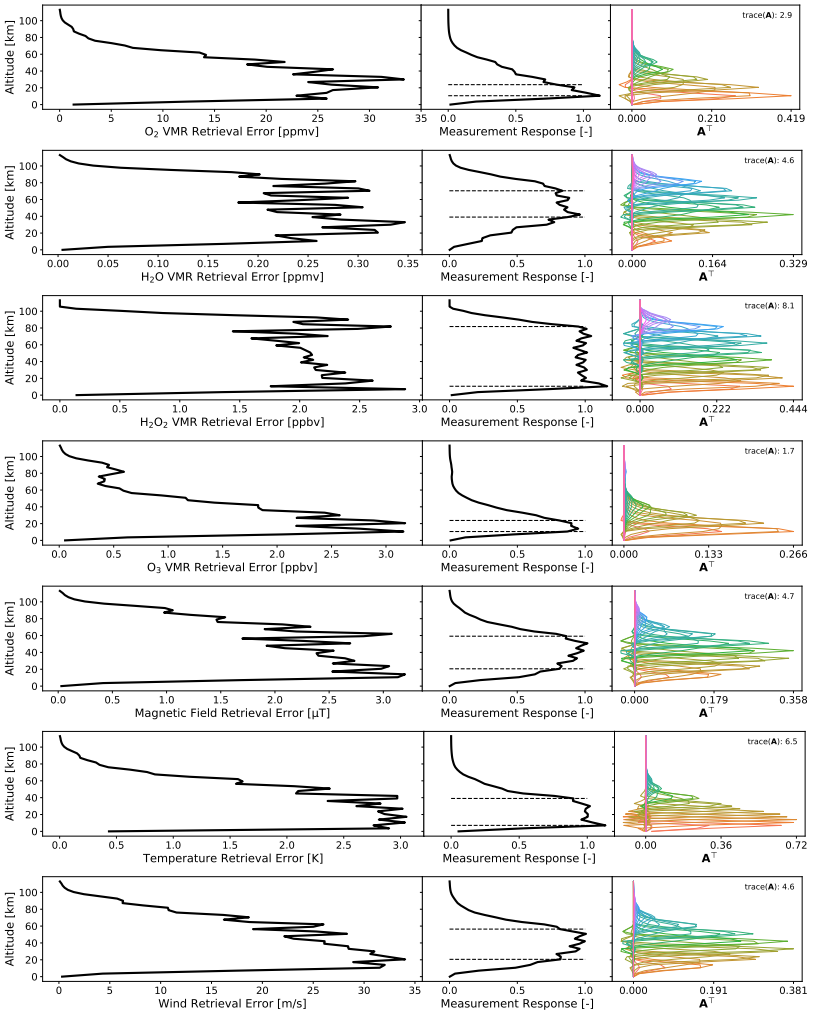

Figure 5. Forward model parameter error estimations for the atmosphere of Figure 2 in limb scanning mode with 1 s integration time at each of the tangent altitudes of Figure 4. By columns, the left column shows the total error estimations and these errors, the central column shows the measurement response by the solid line with the dashed lines marking the 0.8 level, and the right column shows the transpose of the averaging kernel, color coding its columns and showing its trace or the degrees of freedom of the setup. The rows show the forward model parameters whose retrieval are being simulated, with the top row showing molecular oxygen, the second row showing gaseous water, the third row showing hydrogen peroxide, the fourth row showing ozone, the fifth row showing magnetic field, the sixth row showing temperature, and the last row showing wind speed.

– Ozone: The instrument is not sensitive to ozone in nadir staring mode. In limb scanning mode, the error is expected to be about 2 ppbv. For the wet atmosphere, the good measurement response range is limited to from 10 km to 30 km. The dry atmosphere offers a much greater responsive measurement range from 10 km to 60 km. The wet atmosphere scenario has about 50 ppbv in an altitude range around 50 km, so an error at 2 ppbv is good enough to see variations at high altitudes.

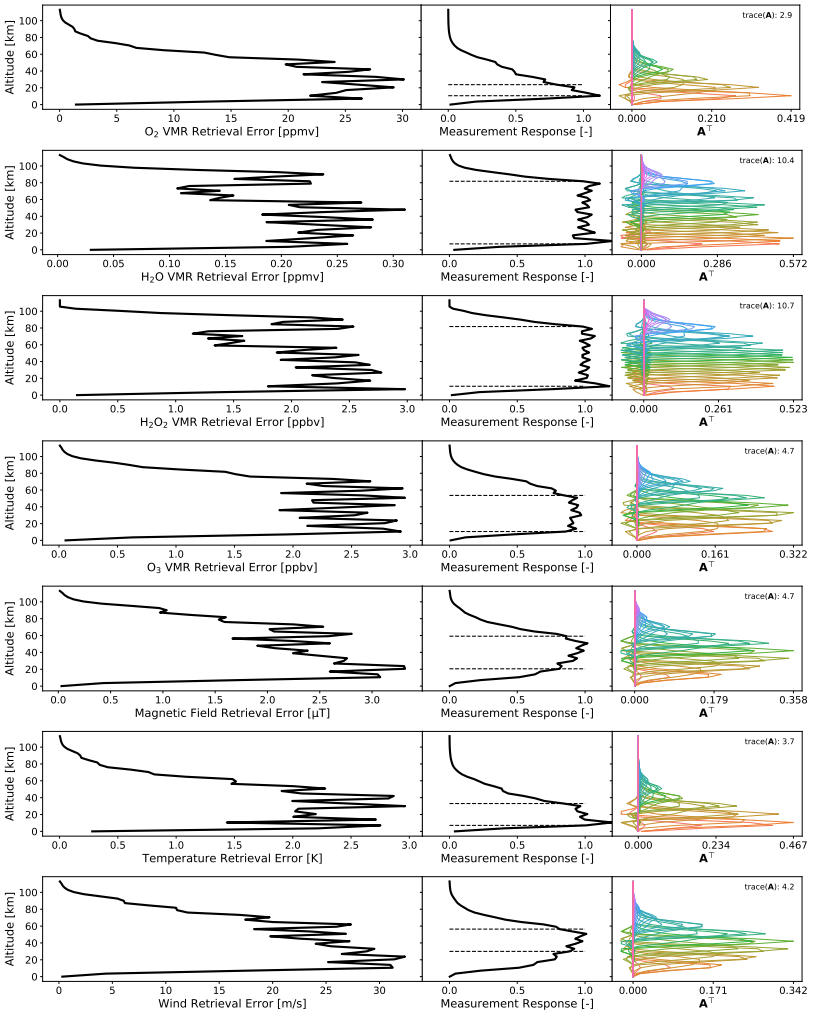

Figure 6. Same as Figure 5 but with gaseous water, hydrogen peroxide, and ozone lowered by a factor 100 to the atmosphere of Figure 2 and a magnetic field strength of $10\,\mathrm{nT}$. Also, molecular oxygen is left out of this figure because it is not affected by the change.

Closer to the surface the ozone mixing ratio increases to above 100 ppbv, but our instrument will only be sensitive for a single profile measurement at those altitudes if the atmosphere is dry and we keep the current constraints. It is possible to be sensitive, e.g., by increasing the standard deviation of ozone in the a priori matrix by one order of magnitude. Doing that, the estimate error increase to about 25 ppbv and near-surface altitudes have good measurement response.

– Magnetic field strength: The error is not affected by the wetness of the atmosphere. For the limb scanning mode scenario, the estimated error is about $2.5\,\mu\mathrm{T}$ in the altitude range from $20\,\mathrm{km}$ to $60\,\mathrm{km}$. In nadir staring mode the error is expected at $1.5\,\mu\mathrm{T}$ from $20\,\mathrm{km}$ to $50\,\mathrm{km}$. Note that the magnetic field is not changing over time but is from sources frozen into the crust. So many subsequent orbits can be used to limit the strength of the magnetic field more strongly. The sensor

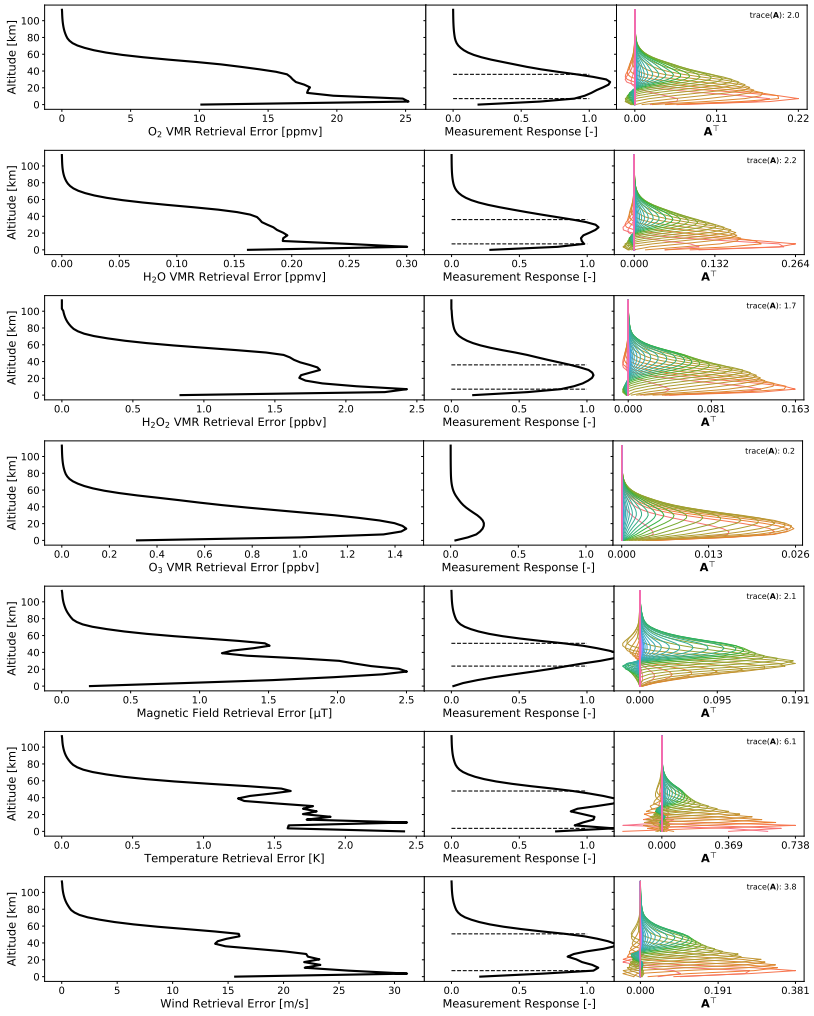

Figure 7. Same as Figure 5 but for nadir staring mode and for one hour of integration time.

measures circular polarization, so only when the magnetic field is pointing at the sensor will there be a strong signal. For nadir staring mode, this limits us to the stronger magnetic field areas, which covers a relatively small area. So to achieve the error here, very many subsequent orbits must observe the area. For limb scanning mode, combining the measurements above a single tangent profile from different azimuth angles will improve the precision even more than shown in our figures. Finally, the molecular oxygen profile in our simulations consists of almost $50\,\%$ less molecular oxygen than has previously been measured because these are produced by the circulation model. A $40\,\%$ increase in molecular oxygen in our simulations means that the estimated error is reduced by about a third of the error estimates given here.

- Temperature: In limb scanning mode, the temperature error estimated for a single profile is about $2\,\mathrm{K}$ to $2.5\,\mathrm{K}$ with good measurement response from $10\,\mathrm{km}$ to $40\,\mathrm{km}$. In nadir staring mode, the temperature error estimation is about $1.5\,\mathrm{K}$ with good measurement response from ground to $50\,\mathrm{km}$.

- Wind speed: The wind speed error is estimated from $20\,\mathrm{ms}^{-1}$ to $25\,\mathrm{ms}^{-1}$ depending on atmospheric wetness, for good measurement response at an altitude range approximately from $20\,\mathrm{km}$ to $60\,\mathrm{km}$. In nadir staring mode, wind speed errors are about $20\,\mathrm{ms}^{-1}$ with good measurement response from $10\,\mathrm{km}$ to $60\,\mathrm{km}$. The vertical wind speed will not be this strong along the path of observations in nadir staring mode, so attempting to retrieve the wind parameter with our instrument in nadir observations will not be useful.

3.3 On Vertical Resolution v. Precision

An estimation of the vertical resolution versus precision can be had by letting the correlation distance increase to large distances. In Figure 8 we let the correlation distance vary from a diagonal a priori matrix to $1000\,\mathrm{km}$ for both nadir staring and limb scanning simulations. The figure also shows the degrees of freedom of of the averaging kernel at these correlation distances, mostly to indicate that what we are trading for increased precision is lower degrees of freedom. The lower correlation distance has already been discussed above so below we only discuss the upper range. The upper range represents a scenario where we assume that the state of the atmosphere at one level is highly correlated to that at every other level. This is a somewhat crude way to reduce the degrees of freedom of the problem and thereby estimate the error at a lower vertical resolution, though it should be sufficient for our purposes. For molecular oxygen, this highly correlated state reduces the estimated errors in the nadir staring mode to about 10 ppmv, and in the limb scanning mode to about 15 ppmv. For gaseous water, the highly correlated state reduces the error estimation to 0.1 ppmv for both nadir staring and limb scanning mode. For hydrogen peroxide, the estimated errors are reduced in the highly correlated state to about 1 ppbv in nadir staring and to 0.5 ppbv in limb scanning mode. The limb scanning mode retains more than one degree of freedom. For ozone, limb scanning mode errors remain at about 2 ppbv in the highly correlated state as its degrees of freedom are low to begin with for the uncorrelated a priori covariance matrix. The magnetic field in the highly correlated state has limb scanning mode estimated errors at $1\,\mu\mathrm{T}$ and in nadir staring at $0.5\,\mu\mathrm{T}$. The temperature error estimation in the highly correlated case retains degrees of freedom in both nadir staring and in limb scanning mode, meaning the retrieval system does not allow the trade that we are after. The errors are expected to be about $1\,\mathrm{K}$. The wind speed also retains degrees of freedom in both viewing geometries. The errors are expected to be around $10\,\mathrm{ms}^{-1}$. Since the magnetic field is highly correlated with distance, these numbers might better represent the precision at which we can retrieve the magnetic field strength than the errors estimated in the previous subsection. For the other parameters, the correlation distances are too long so the number represents a limit at poor vertical resolution for a single profile measurement.

4 Conclusions

We present a feasibility study for a sub-millimeter instrument on a small Mars mission currently under construction. The instrument will be able to measure several atmospheric species crucial for understanding Martian molecular oxygen, gaseous

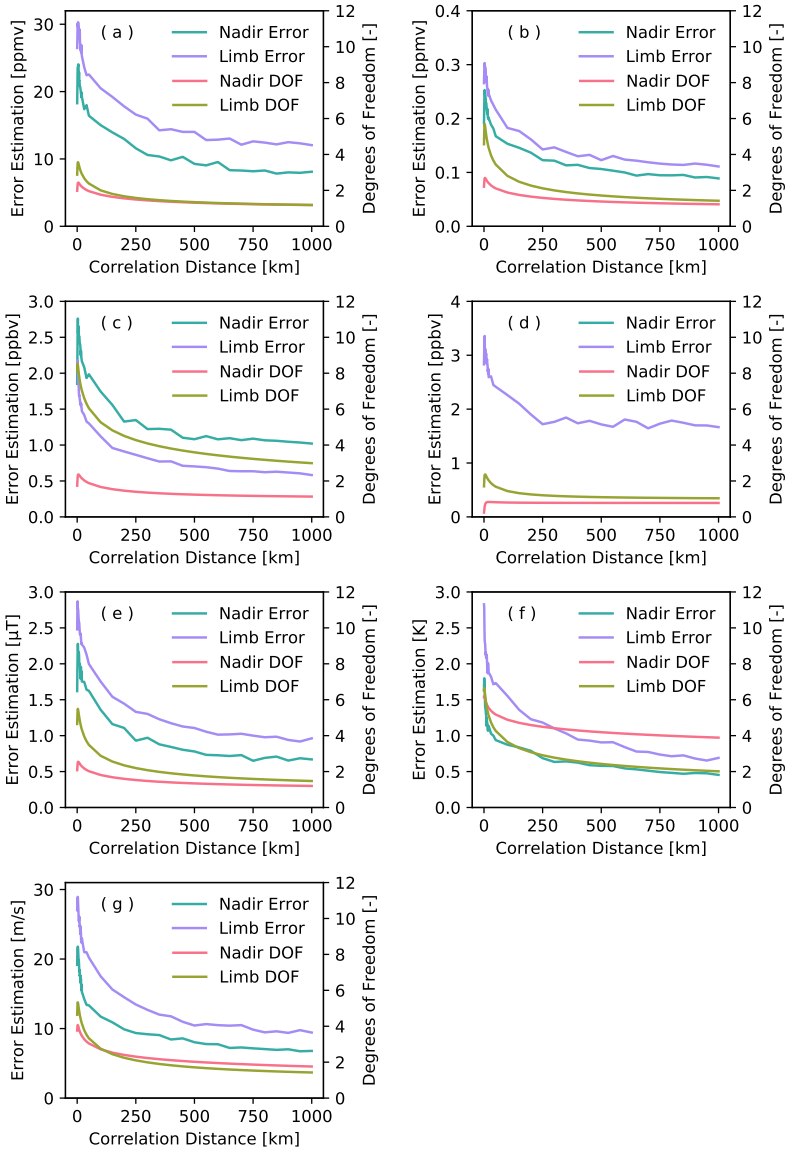

Figure 8. Correlation distance versus estimated errors and degrees of freedom (DOF). Panel (a) is for molecular oxygen. Panel (b) is for gaseous water. Panel (c) is for hydrogen peroxide. Panel (d) is for ozone. Panel (e) is for the magnetic field strength. Panel (f) is for the temperature. Panel (g) is for the wind speed. Legends indicate if the line belongs to the right y-axis or left y-axis, as well as the observation strategy as used for Figures 5 or 7. The estimated errors are the mean over the range of $\max(\mathbf{r}) > 0.8$, so the ozone-panel lacks a line for nadir staring mode since it is never sensitive at the a priori standard deviations presented in the subsection on error analysis.

water, hydrogen peroxide, and ozone at low errors. In addition to these, the instrument will be able to limit the crustal magnetic field, and get the meteorological parameters of temperature and wind speed. The expected measurement errors before spatial

and temporal averaging are 15 ppmv to 25 ppmv for the molecular oxygen mixing ratio, 0.2 ppmv for the gaseous water mixing ratio, 2 ppbv for the hydrogen peroxide mixing ratio, 2 ppbv for the ozone mixing ratio, $1.5\,\mu\mathrm{T}$ to $2.5\,\mu\mathrm{T}$ for the magnetic field strength, $1.5\,\mathrm{K}$ to $2.5\,\mathrm{K}$ for the temperature profile, and $20\,\mathrm{m\,s^{-1}}$ to $25\,\mathrm{m\,s^{-1}}$ for the horizontal wind speed. These error ranges are well within the range to push the boundary of Mars knowledge.

References

Atreya, S., Wong, A.-S., Renna, N., Farrell, W., Delory, G., Sentman, D., Cummer, S., Marshall, J., Rafkin, S., and Catling, D.: Oxidant Enhancement in Martian Dust Devils and Storms: Implication for Life and Habitability, Astrobiology, 6, 439–450, 2006.

Buehler, S. A., Mendrok, J., Eriksson, P., Perrin, A., Larsson, R., and Lemke, O.: ARTS, the Atmospheric Radiative Transfer Simulator – version 2.2, the planetary toolbox edition, Geoscientific Model Development, 11, 1537–1556, https://doi.org/10.5194/gmd-11-1537-2018, https://www.geosci-model-dev.net/11/1537/2018/, 2018.

Carleton, N. P. and Traub, W. A.: Detection of molecular oxygen on Mars, Science, 177, 988–992, 1972.

Delory, G., Farrell, W., Atreya, S., Renna, N., Wong, A.-S., Cummer, S., Sentman, D., Marshall, J., Rafkin, S., and Catling, D.: Oxidant Enhancement in Martian Dust Devils and Storms: Storm Electric Fields and Electron Dissociative Attachment, Astrobiology, 6, 450–462, 2006.

Eriksson, P., Jiménez, C., and Buehler, S. A.: Qpack, a general tool for instrument simulation and retrieval work, Journal of Quantitative Spectroscopy and Radiative Transfer, 91, 47–64, https://doi.org/10.1016/j.jqsrt.2004.05.050, 2005.

Eriksson, P., Buehler, S. A., Davis, C. P., Emde, C., and Lemke, O.: ARTS, the atmospheric radiative transfer simulator, Version 2, Journal of Quantitative Spectroscopy and Radiative Transfer, 112, 1551–1558, 2011.

Forget, F., Hourdin, F., Foumier, R., Hourdin, C., and Talagran, O.: Improved general circulation models of the Martian atmosphere from the surface to above 80 km, Journal of Geophysical Research, 104, 155–175, 1999.

Gruszka, M. and Borysow, A.: Roto-Translational Collision-Induced Absorption of CO2for the Atmosphere of Venus at Frequencies from 0 to 250 cm1, at Temperatures from 200 to 800 K, Icarus, 129, 172–177, https://doi.org/https://doi.org/10.1006/icar.1997.5773, 1997.

Hartogh, P.: High-resolution chirp transform spectrometer for middle atmospheric microwave sounding, https://doi.org/10.1117/12.301141, http://dx.doi.org/10.1117/12.301141, 1997.

Hartogh, P., Jarchow, C., Lellouch, E., Val-Borro, M., Rengel, M., Moreno, R., Medvedev, A., Sagawa, H., Swinyard, B., Cavalié, T., Lis, D., Błęcka, M., Banaszkiewicz, M., Bockelée-Morvan, D., Crovisier, J., Encrenaz, T., Küppers, M., Lara, L., Szutowicz, S., Vandenbussche, B., Bensch, F., Bergin, E. A., Billebaud, F., Biver, N., Blake, G., Blommaert, J., Cernicharo, J., Decin, L., Encrenaz, P., Feuchtgruber, H., Fulton, T., de Graauw, T., Jehin, E., Kidger, M., Lorente, R., Naylor, D., Portyankina, G., Sánchez-Portal, M., Schieder, R., Sidher, S., Thomas, N., Verdugo, E., Waelkens, C., Whyborn, N., Teyssier, D., Helmich, F., Roelfsema, P., Stutzki, J., LeDuc, H., and Stern, J.: Herschel/HIFI observations of Mars: first detection of O_2 at submillimetre wavelengths and upper limits on HCl and H_2O_2, Astronomy & Astrophysics, 521, L49, https://doi.org/10.1051/0004-6361/201015160, 2010.

Kasai, Y., Sagawa, H., Kuroda, T., Manabe, T., Ochiai, S., Kikuchi, K., Nishibori, T., Baron, P., Mendrok, J., Hartogh, P., Murtagh, D., Urban, J., von Schéele, F., and Frisk, U.: Overview of the Martian atmospheric submillimetre sounder FIRE, Planetary and Space Science, 63-64, 62–82, 2012.

Larsson, R., Lankhaar, B., and Eriksson, P.: Updated Zeeman effect splitting coefficients for molecular oxygen in planetary applications. Under preparation.

Larsson, R., Ramstad, R., Mendrok, J., Buehler, S. A., and Kasai, Y.: A Method for Remote Sensing of Weak Planetary Magnetic Fields: Simulated Application to Mars, Geophysical Research Letters, 40, 5014–5018, 2013.

Larsson, R., Buehler, S. A., Eriksson, P., and Mendrok, J.: A treatment of the Zeeman effect using Stokes formalism and its implementation in the Atmospheric Radiative Transfer Simulator (ARTS), Journal of Quantitative Spectroscopy and Radiative Transfer, 133, 445–453, 2014.

Larsson, R., Milz, M., Eriksson, P., Mendrok, J., Kasai, Y., Buehler, S. A., Diéval, C., Brain, D., and Hartogh, P.: Martian magnetism with orbiting sub-millimeter sensor: simulated retrieval system, Geoscientific Instrumentation, Methods and Data Systems, 6, 27–37, 2017.

Mahaffy, P. R., Webster, C. R., Atreya, S. K., Franz, H., Wong, M., Conrad, P. G., Harpold, D., Jones, J. J., Leshin, L. A., Manning, H., Owen, T., Pepin, R. O., Squyres, S., Trainer, ., and Team, M. S.: Abundance and Isotopic Composition of Gases in the Martian Atmosphere from the Curiosity Rover, Science, 341, 263–266, 2013.

Rodgers, C. D.: Inverse methods for atmospheric sounding: Theory and practice, vol. 2, World Scientific Publishing Co. Pte. Ltd., 2000.

Sandel, B., Gröller, H., Yelle, R., Koskinen, T., Lewis, N., Bertaux, J.-L., Montmessin, F., and Quémerais, E.: Altitude profiles of O_2 on Mars from {SPICAM} stellar occultations, Icarus, 252, 154–160, https://doi.org/http://dx.doi.org/10.1016/j.icarus.2015.01.004, 2015.

Urban, J., Dassas, K., Forget, F., and Ricaud, P.: Retrieval of vertical constituents and temperature profiles from passive submillimeter wave limb observations of the Martian atmosphere: a feasibility study, Appl. Opt., 44, 2438–2455, https://doi.org/10.1364/AO.44.002438, http://ao.osa.org/abstract.cfm?URI=ao-44-12-2438, 2005.

Zeeman, P.: On the Influence of Magnetism on the Nature of the Light Emitted by a Substance, Astrophysical Journal, 5, 332–347, https://doi.org/10.1086/140355, 1897.